INSTITUTE OF PHYSICS PUBLISHING SMART MATERIALS AND STRUCTURES
Smart Mater. Struct. **15** (2006) 1919–1926 doi:10.1088/0964-1726/15/6/048

Design of a recurve actuator for maximum energy efficiency

Omprakash Seresta[1], Scott Ragon[2], Mostafa M Abdalla[3], Zafer Gürdal[3] and Douglas K Lindner[4]

[1] Department of Aerospace and Ocean Engineering, Virginia Polytechnic Institute and State University, Blacksburg, VA 24061, USA
[2] Phoenix Integration, Incorporated, 1715 Pratt Drive, Suite 2000, Blacksburg, VA 24060, USA
[3] Aerospace Structures, Faculty of Aerospace Engineering, Delft University of Technology, Delft, The Netherlands
[4] Bradley Department of Electrical and Computer Engineering, Virginia Polytechnic and State University, Blacksburg, VA 24061, USA

Received 22 February 2006, in final form 21 September 2006
Published 13 November 2006
Online at stacks.iop.org/SMS/15/1919

Abstract
In this paper we study the optimal design of recurve arrays. An analytic model of the static response of the recurve actuator with energy flow in the system is derived. Two optimization problems for the recurve array are formulated with material, packaging, and performance constraints. One formulation is based on minimum weight. The second formulation is based on energy efficiency. A genetic algorithm is used to find the optimum designs. Recurve arrays designed for maximum energy conversion efficiency are compared to those designed for minimum weight. Parametric studies are conducted to investigate the effect of the stiffness of the driven structure and the maximum deliverable voltage on the optimized designs. These optimization formulations are effective design tools for a relatively complex actuator.

(Some figures in this article are in colour only in the electronic version)

Nomenclature

b	width of a recurve bimorph
b_a	normalized recurve array width
b^*	width specification of the recurve array
c	capacitance per unit length
C^b	clamped capacitance of a recurve bimorph
C^F	free force capacitance of the PZT
C^δ	zero displacement capacitance
CS	recurve connection stiffness
d_{13}	PZT material coupling coefficient between axial and poling direction
δ	displacement of the recurve bimorph
δ_a	normalized recurve array displacement
δ_f	displacement at the center of the recurve array
δ_f^*	free displacement specification for the recurve array
Δ^F	free displacement per volt
Δ^V	short circuit compliance
s_{33}	free electrical permittivity of the PZT material
E_a	normalized electric field
E_e	input electrical energy
E_g	maximum electric field set up by the amplifier
E_m	output mechanical energy
EI^V	short circuit bending stiffness
f_r	stiffness reduction factor due to finite recurve connection stiffness
F	applied external force
F_a	normalized block force on the recurve array
F_b^*	blocked force specification for the recurve array
h	height of the recurve array
h_a	normalized height of the recurve array
h^*	height specification of the recurve array
η	energy efficiency
k	piezoelectric coupling coefficient
$\bar{k}$	equivalent coupling coefficient
K	stiffness of the load spring
κ	beam curvature
l	length of a recurve bimorph
L_a	normalized recurve array length

L^*	length specification of the recurve array
m	number of parallel elements in the recurve array
M	bending moment
M_0	support reaction moment
μ	induced piezoelectric moment per volt
n	number of series element in the recurve array
q	net charge flowing into the array
r	number of layers in the PZT multimorph
R	ratio of array stiffness to the load stiffness
ρ_p	density of the PZT material
ρ_b	density of the beam substrate material
t_a	total thickness of the PZT layers
t_b	thickness of the substrate
t_p	thickness of each PZT layer
t_s	spacing between two series recurve elements
V	voltage applied to the array
V_g	maximum voltage delivered by the drive amplifier
$w(x)$	transverse displacement of the recurve bimorph
W	weight of the recurve array
x	poling direction
Y_a	open circuit Young's modulus of PZT material
Y_b	Young's modulus of the substrate
Y_{11}	Young's modulus of the PZT material in poling direction

1. Introduction

Smart materials and smart structures have received substantial interest in the past decade due to their broad applications in areas of aerospace, manufacturing, defense, and civil infrastructure systems, to name a few. The trend in smart actuators has been to include the active materials in ever more complex mechanisms so that the resultant smart actuator matches the force and displacement requirements of the applications of interest. One example of such an actuator is the recurve array (Ervin and Brei 1998a), shown in figure 1.

One of the design challenges of this new generation of actuator is their relative complexity. Recently, design optimization has emerged as a design tool for smart actuators. As demonstrated in a number of other studies (Abdalla *et al* 2003, Busquets-Monge *et al* 2004, Chandrasekaran *et al* 2000, Chandrasekaran and Lindner 2000, Lindner *et al* 2001, Frecker 2002) mathematical optimization techniques offer an organized and methodical way of formulating and solving the design problem. This approach allows the designer to potentially use a large number of design variables and fewer simplifications in modeling the system. Better models, in turn, may reduce the number of iterations during the hardware-testing phase. The increasing speed of computer hardware and the development of faster computational models allow optimum designs to be obtained in a relatively short time. Furthermore, the application of the optimization techniques can provide a better understanding of the tradeoffs involved in the design, and may even highlight those trends that are not obvious.

In this work, we focus our attention on the recurve array proposed by Ervin and Brei (1998a). Using this actuation building block, parallel and serial connection for piezoceramic recurve actuator arrays are demonstrated by Ervin and Brei (1998b). Several models are proposed to study the behaviour

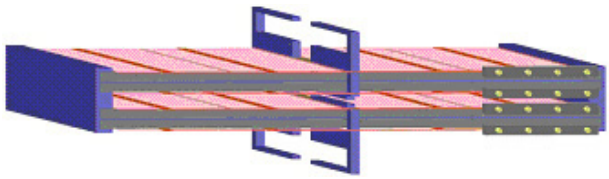

Figure 1. Recurve element (Ervin and Brei 1998a).

of piezoceramic materials (Kamlah and Jiang 1999, Lu and Hanagud 2002, Smith and Ounaies 2000). Recently, Ervin and Brei (2004) studied the dynamic response of piezoelectric recurve actuation architectures. To the authors' knowledge no attempt has been made to take into account the energy flow in the analysis model, which is crucial to applications with limited power supply. The recurve array is a good candidate for design optimization because it has many design variables, both continuous and discrete. Because this is a mixed optimization problem we used a genetic algorithm (Nagendra *et al* 1996). We formulated the objective function in two ways. First, we define the optimization problem as a weight minimization problem. This formulation is appropriate for applications where weight and/or volume specifications are critical. Second, we define the optimization problem as an efficiency maximization problem. This formulation is appropriate for applications where the power source has limited capacity. Many components of a smart structural system contribute to and influence the energy efficiency of the overall system (Abdalla *et al* 2005). Apart from energy losses in the actuator and the drive electronics, an important consideration is the energy conversion efficiency of the actuator. Even when the drive electronics and the actuator are completely free from energy dissipation, only a limited fraction of the energy supplied by the electric circuit will be deliverable to the controlled structure. The rest of the energy will be stored in the actuator. Since all the input energy to drive the actuator will have to be supplied by the electronics, energy conversion efficiency plays a key role in determining the overall size of the system.

The optimization formulation developed in the paper also allows for a numerical study of the interaction between the drive electronics and the complexity of the recurve array. As the maximum voltage that the drive amplifier can deliver is decreased, the complexity of the recurve array increases. Conversely, as the maximum voltage increases, the recurve array looks more and more like a single piece of PZT. Since high voltage amplifiers are more complex than their low voltage counterparts, we see an interesting trade between the size and complexity of the mechanical part of the actuator and the size and complexity of the drive electronics.

In the following section, we first provide a description of the recurve actuator, followed by an analytic study of energy flow from the drive circuit through the actuator to the structure. The structure is modeled as a linear spring, and we consider static response only. The optimization problem is then formulated, and the genetic algorithm (GA) used is briefly described. Optimal designs are obtained for minimum weight and for maximum energy conversion efficiency. Numerical parametric studies are carried out to investigate the effect of maximum deliverable voltage and the structure stiffness on these optimum designs.

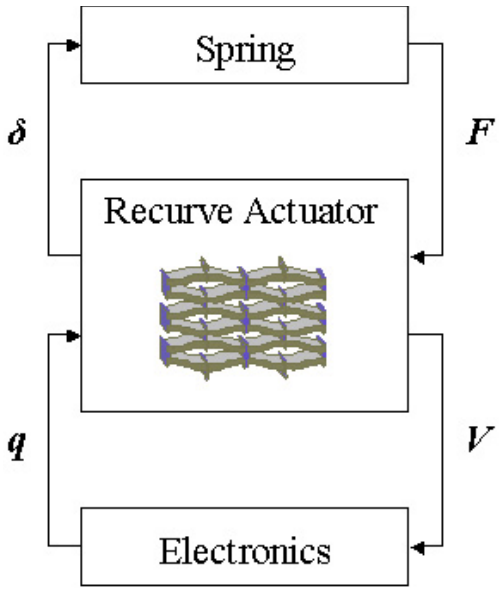

Figure 2. Smart actuator.

2. Recurve actuator

The smart actuator configuration that uses an array of recurve actuators considered in this paper is shown in figure 2. The central component of this actuator is a recurve array (Ervin and Brei 1998a) of figure 1. It is this component on which we will focus our attention. The mass/spring system provides a load for the recurve array. Here we assume that the load is a spring with stiffness K. The electronic amplifier provides the electric power to drive the recurve array. We assume that the amplifier can deliver a maximum voltage of V_g. The amplifier and the load provide boundary conditions for the optimization of the recurve array.

As suggested by figure 2, the recurve array is composed of cantilever beams (called here a recurve bimorph) with two pairs of piezoelectric multimorph patches along its length as shown in figure 3. Of course, the recurve bimorph can be constructed of layered piezoelectric material. Figure 4 shows a cross section of the recurve bimorph in figure 3 along with its dimensions.

In figure 3 the four multimorph piezoelectric patches are polled such that the induced moments act in opposite directions over each half of the beam. This geometry causes the beam to bend with positive curvature up to the mid-span and negative curvature over the other half, producing a relative displacement of the end of the beam in a direction perpendicular to the beam axis without relative rotation of the ends. Thus, unlike a straight bender, recurve components can be joined at their free ends to form a recurve couple. Two recurve couple are then joined together to form a recurve element as shown in figure 1. These recurve elements can be interconnected into serial and parallel arrays, without constraining each other from motion. These components are replicated and assembled together into a recurve array as shown in figure 2.

A basic feature of the recurve array is the ability to connect a number of basic recurve couples in parallel and/or in series to tailor the design to meet specific displacement and force

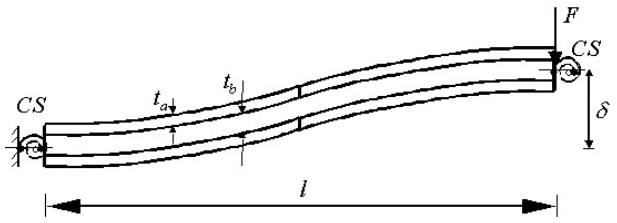

Figure 3. Recurve bimorph.

requirements. By increasing the number of serial elements, larger displacements for the same force can be achieved. By increasing the number of parallel elements, larger forces can be driven for the same displacement requirements.

From this brief description, we can see that the design of a recurve array is relatively complex. Typically, we are given specifications for the recurve array including force/displacement requirements, voltage restrictions from the drive amplifier, and packaging restrictions. Based on these specifications, all of the materials must be selected, the geometry determined, and the dimensions selected. The design includes determining the layering of the bimorphs and the number and arrangement of the recurve elements. In this paper we approach this design problem using mathematical optimization methodologies.

2.1. Modeling of the recurve array

In this section we will develop a static model for the recurve array that is used in the optimization algorithms below. The approach is to develop a 2×2 transfer matrix based on the variables defined in figure 2. This transfer matrix is developed from the equations for a recurve bimorph which are developed first. Finally, an expression for the efficiency of the recurve array is derived.

2.1.1. Single recurve bimorph. The constitutive equations of an active beam are given by (Busquets-Monge *et al* 2004),

$$M = EI^V \kappa - \mu V \tag{1}$$

$$\frac{\mathrm{d}q}{\mathrm{d}x} = cV + \mu\kappa. \tag{2}$$

For the recurve geometry as defined in figures 3 and 4, the EI^V, μ, and c, are defined in terms of the geometric and material properties of the beam in the following form (Abdalla *et al* 2003)

$$EI^V = \frac{b}{12}\left[Y_b t_b^3 + 2Y_a t_a \left(4t_a^2 + 6t_a t_b + 3t_b^2\right)\right] - k^2 \frac{b}{2} Y_a t_a [(t_a + t_b)^2 + (r^2 - 1)t_a^2/3r^2] \tag{3}$$

$$\mu = r\left(1 - k^2\right) d_{13} Y_a b\,(t_a + t_b) \tag{4}$$

$$c = 2r^2 \varepsilon_{33}\left(1 - k^2\right)\frac{b}{t_a}. \tag{5}$$

The open circuit Young's modulus of the PZT material Y_a is given by

$$Y_a = \frac{Y_{11}}{1 - k^2}. \tag{6}$$

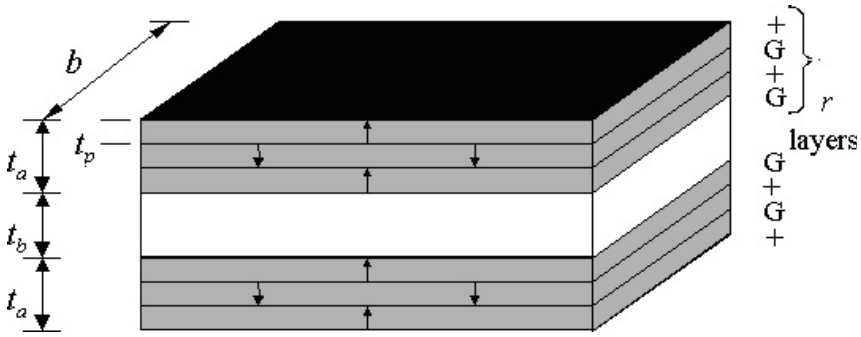

Figure 4. Dimensions of the cross sections of a recurve bimorph.

The PZT material electromechanical coupling coefficient k^2 is

$$k^2 = \frac{Y_{11} d_{13}^2}{\varepsilon_{33}}. \tag{7}$$

In order to determine the output displacement and force characteristics of the actuator, we solve for the beam transverse displacements using small deflections assumption. The bending curvature in this case is given by

$$\kappa = \frac{\mathrm{d}^2 w(x)}{\mathrm{d}x^2} \tag{8}$$

and the bending moment distribution from statics is

$$M = M_0 - F(l - x). \tag{9}$$

Solving the bending curvature from equation (1), and using equation (9), we obtain

$$\frac{\mathrm{d}^2 w(x)}{\mathrm{d}x^2} = \frac{1}{EI^V} \begin{cases} \mu V + M_0 - F(l-x) & 0 < x < l/2 \\ -\mu V + M_0 - F(l-x) & l/2 < x < l. \end{cases} \tag{10}$$

Note that the PZT induced bending moments change sign in equation (10) between the first and second half of the beam. Equation (10) is integrated twice to obtain the deflected shape $w(x)$. The constants of integration and the value of the support reaction M_0 are obtained from the boundary conditions

$$\begin{aligned} w(x)|_{x=0} &= 0 \\ CS \left.\frac{\mathrm{d}w(x)}{\mathrm{d}x}\right|_{x=0} &= M_0 \\ CS \left.\frac{\mathrm{d}w(x)}{\mathrm{d}x}\right|_{x=l} &= -M_0. \end{aligned} \tag{11}$$

The recurve connection stiffness is expressed in terms of cross section dimensions as (Abdalla *et al* 2003)

$$CS = \frac{b}{5.3}\left[Y_a t_a (t_a + t_b) + \frac{1}{2} Y_b t_b^2\right]. \tag{12}$$

Given the beam displacements $w(x)$, we can determine the deflection of the beam at the free end $\delta = w(l)$ in terms of the applied voltage, external force, and stiffness and properties of the beam as

$$\delta = \begin{bmatrix} \frac{(1+6f_r)l^3}{EI^V} & \frac{\mu l^2}{4EI^V} \end{bmatrix} \begin{Bmatrix} F \\ V \end{Bmatrix}. \tag{13}$$

The stiffness reduction factor due to the finite recurve connection stiffness f_r given by

$$f_r = 1 + \frac{6EI^V}{CSl}. \tag{14}$$

We next substitute the definition of the curvature and the displacement expression into equation (2) and, assuming constant piezoelectric moment, μ, and capacitance, c, integrate equation (2) over the beam length to determine the net charge as a function of the applied voltage, external force, and stiffness and properties of the beam. Finally, we reach a 2×2-matrix relationship with net tip displacement and charge as output variables and the applied force and voltage as inputs.

$$\begin{Bmatrix} \delta \\ q \end{Bmatrix} = \begin{bmatrix} \frac{(1+6f_r)l^3}{EI^V} & \frac{\mu l^2}{4EI^V} \\ \frac{\mu l^2}{4EI^V} & C^F \end{bmatrix} \begin{Bmatrix} F \\ V \end{Bmatrix}. \tag{15}$$

In equation (15) the recurve free force capacitance given by

$$C^F = \left(c + \frac{\mu^2}{EI^V}\right) l. \tag{16}$$

It is also useful to define the free displacement (displacement at zero force) per unit voltage as

$$\Delta^F = \frac{\mu l^2}{4EI^V} \tag{17}$$

and the short circuit compliance

$$\Delta^V = \frac{(1+6f_r)\,\mu l^3}{12EI^V}. \tag{18}$$

We also define clamped capacitance of a recurve element C^δ as the capacitance when the displacement is restricted to zero, which can be expressed as

$$C^\delta = C^F - \frac{(\Delta^F)^2}{\Delta^V}. \tag{19}$$

Thus, an equivalent coupling coefficient $\bar{k}^2$ for the recurve bimorph can be defined similar to electromechanical coupling coefficient of the material as

$$\bar{k}^2 = 1 - \frac{C^\delta}{C^F}. \tag{20}$$

2.1.2. Recurve arrays. A recurve array is formed by connecting m recurve bimorphs in parallel and n recurve bimorphs series. For a recurve array the system of equations (15) (using equations (16)–(18)) takes the form

$$\begin{Bmatrix} \delta \\ q \end{Bmatrix} = \begin{bmatrix} \frac{n}{m}\Delta^V & n\Delta^V \\ n\Delta^V & nmC^F \end{bmatrix} \begin{Bmatrix} F \\ V \end{Bmatrix}. \tag{21}$$

2.2. Energy analysis

Next we derive an expression for the efficiency of a recurve array. For this analysis we assume that the recurve array is used to deflect a linear output spring of stiffness K. Then we have $F = K\delta$. With this assumption the deflection–force relations in equation (15) can be solved for the force, deflection, and net charge responses in terms of the applied voltage as

$$\delta = \frac{mn\Delta^F}{m + n\Delta^V K} V \tag{22}$$

$$F = \frac{mnK\Delta^F}{m + n\Delta^V K} V \tag{23}$$

$$q = mnC^F \left(\frac{m + nK\Delta^V(1 - \bar{k}^2)}{m + nK\Delta^V} \right) V. \tag{24}$$

The electrical energy delivered by the amplifier is

$$E_e = \tfrac{1}{2} q V. \tag{25}$$

The energy delivered to the mechanical load is

$$E_m = \tfrac{1}{2} \delta F. \tag{26}$$

Thus, the energy efficiency, defined as the output mechanical energy (equation (26)) divided by the input electrical energy (equation (25)), can be found using equations (22)–(24) as,

$$\eta = \frac{E_m}{E_e} = \frac{\bar{k}^2 R}{(1 + R)\left[1 + R(1 - \bar{k}^2)\right]} \tag{27}$$

where R is the ratio of structural stiffness to recurve array stiffness given by,

$$R = \frac{nK\Delta^V}{m} = \frac{K}{\frac{m}{n\Delta^V}}. \tag{28}$$

It is concluded from equation (27) that the overall energy conversion efficiency depends on how much energy can be converted by a recurve element through $\bar{k}^2$. It also depends on the matching of the actuator stiffness to the structure stiffness through R. Similar conclusions were found in Abdalla *et al* (2003) for a structure actuated by a combination of a PZT stack and a compliant mechanism.

Other important performance measures are the blocked force and the free displacement, which are used in the optimization algorithm below. The free displacement can be obtained by setting $K = 0$ in equation (22). We have

$$\delta_f = n\Delta^F V. \tag{29}$$

The blocked force is obtained by taking the limit as K tends to infinity in equation (23). This calculations yields,

$$F_b = m\frac{\Delta^F}{\Delta^V} V. \tag{30}$$

3. Optimization formulation

3.1. Objective function

Here we consider two objective functions for the optimization formulation. The first objective function is the recurve array weight

$$\min_{\text{design var}} W \tag{31}$$

where the weight is given by

$$W = 2lbmn\left(2rt_p\rho_p + t_b\rho_b\right). \tag{32}$$

This formulation is suitable for applications where the actuator has strict weight and/or volume constraints.

The second objective function is the efficiency of the recurve array

$$\max_{\text{design var}} \eta. \tag{33}$$

The formulation is motivated by applications where the energy supply is limited, and it is desirable to extend the lifetime operation of the system. For example, these applications may have only a battery as a power source (Brei *et al* 2003).

3.2. Constraints

The same constraints are used for both objective functions. The first constraint is on the blocked force

$$F_a = \frac{F_b}{F_b^*} \geqslant 1 \tag{34}$$

where F_b is given by equation (30), and F_b^* is the user-specified minimum blocked force. The second constraint is on the minimum displacement

$$\delta_a = \frac{\delta_f}{\delta_f^*} \geqslant 1 \tag{35}$$

where δ_f is given by equation (29). The third set of constraints are defined by a user-specified volume. These constraints can be expressed as

$$\begin{aligned} L_a &= \frac{2ml}{L^*} \leqslant 1 \qquad b_a = \frac{b}{b^*} \leqslant 1, \\ h_a &= \frac{n\left(2rt_p + t_b\right) + (n-1)t_s}{h^*} \leqslant 1. \end{aligned} \tag{36}$$

In this calculation it is assumed that the spacing between two series recurve elements t_s is to be twice the maximum displacement of an individual recurve bimorph $t_s = 2\delta_f/n$.

The fourth constraint is imposed by the drive amplifier which we assume can supply a maximum drive voltage V_g. When this maximum voltage is applied to a piezoelectric material it sets up a field

$$E_g = \frac{V_g}{t_p}. \tag{37}$$

We do not want this field to depole the individual layer of piezoelectric material. Hence, given the maximum voltage from the drive amplifier and given the saturation field of the piezoelectric material E_c, these constraints impose a maximum

Table 1. Design variables.

Design variable	Type	Description
n	Integer	No. of series elements
m	Integer	No. of parallel elements
r	Integer	No. of PZT layers
l	Continuous	Recurve length
b	Continuous	Recurve width
t_b	Continuous	Beam substrate thickness
t_p	Continuous	PZT layer thickness

Table 2. Design specifications.

F_b^*	δ_f^*	L^*	b^*	h^*
30 N	500 μm	150 mm	25 mm	35 mm

limitation on the thickness of the piezoelectric material. This constraint can be expressed as

$$E_a = \frac{V^*}{E_c t_p} \leqslant 1. \tag{38}$$

All of these constraints are typical design specifications for actuators.

3.3. Design variables

The design variables consist of the geometry, dimensions, and materials of the recurve array. The geometry of the array is the number of series and parallel elements. The dimensions of the array are determined by the dimensions of the recurve bimorph including the length, width, and thickness of the substrate. The other dimensions of the bimorph include the number of layers of the piezoelectric material as well as their thickness. These design variables are summarized in table 1.

Another set of design variables that could be included in this optimization is the selection of the materials in the recurve array including the type of piezoelectric material and the type of core material used in the recurve bimorph. These design variables were not included in the demonstration problems below.

3.4. Optimization algorithm

This optimization problem is characterized by the presence of both continuous and discrete design variables in almost equal numbers. These types of problems pose challenges to the traditional gradient-based algorithms that have been widely applied to solve continuous design variable problems. Other stochastic approaches such as genetic algorithms (GA) have been successfully applied to solve both continuous and discrete design variable problems (Nagendra *et al* 1996). A GA was selected to solve the present problem, in view of its ability to handle integer variables. Moreover, the design space contains a number of local optima, and the stochastic nature of GA increases the possibility of converging to the global optimum design.

4. Results

The performance of this algorithm was demonstrated using the actuator specifications from the Intertially Stablized Rifle (Brei *et al* 2003). The design specifications are given in table 2. The piezoelectric material used is PZT5 and brass is used for the beam substrate. Material properties are listed in table 3. The GA algorithm described in McMahon *et al* (1998) was run using a population size of 200 individuals for 25 000 generations. Multiple Elitist selection was used with a crossover probability of 1.00, and a mutation probability of 0.1.

Table 3. Material properties.

Y_b	106 GPa
Y_{11}	63 GPa
ε_{33}	3.365×10^{-8} C^2 N^{-1} m^{-2}
d_{13}	3.55×10^{-10} m V^{-1}
ρ_p	7450 kg m^{-3}
ρ_b	8542 kg m^{-3}

Recurve array designs optimized for minimum weight are presented in table 4, and designs optimized for maximum energy efficiency are presented in table 5. In each case, results are presented for different values of the structure stiffness and applied voltage. Active constraints are highlighted in *bold* type.

Comparing the weight of designs for different values of structural stiffness in tables 4 and 5, we note that although the structural stiffness does not influence the minimum weight designs, it does have a significant influence on the energy efficiency of these designs. For small values of structural stiffness (1000–10 000 N m^{-1}), optimizing for minimum weight yields designs that are similar in performance to those obtained by optimizing for maximum energy efficiency. The maximum efficiency designs are from 5% to 50% more efficient than the minimum weight designs, but are also from 5% to 50% heavier. Physically, the minimum weight designs are characterized by a zero beam substrate thickness, whereas the maximum efficiency designs have beam substrate thickness that range from 300 to 950 μm and 1–2 fewer PZT layers. The most critical constraints for the both the minimum weight and maximum efficiency designs are the minimum blocked force constraint (equation (34)) and the material saturation constraint (equation (38)). Also, as indicated in tables 4 and 5, the length and width packaging constraints are active for many of the designs.

For larger values of the structural stiffness (100 000–500 000 N m^{-1}), performance differences between the minimum weight and maximum efficiency designs are more pronounced. Compared to the minimum weight designs, the maximum efficiency designs are 25%–50% heavier, but over 500% more efficient. The physical differences described for the low stiffness designs are more pronounced: the minimum weight designs continue to have zero beam substrate thicknesses, whereas the maximum efficiency designs have beam substrate thicknesses that range from 1000 to 1700 μm. The blocked force constraint (equation (34)) is active for the minimum weight designs, whereas the free displacement constraint (equation (35)) is active for the maximum efficiency designs. As before, the length and width packaging constraints are active for many of the designs.

The effect of the maximum applied voltage on the optimal weights and efficiencies appears to be insignificant. The differences that do exist are a result of the discrete nature of

Table 4. Weight optimization results.

K (N m^{-1})	V_g (V)	m	n	r	l (mm)	b (mm)	t_p (μm)	t_b (μm)	E_a	δ_a	F_a	L_a	b_a	h_a	η (%)	W ($\times 10^{-4}$)
500 000	100	2	10	3	37.5	22.78	250	0.0	**1.00**	3.96	1.05	**1.00**	0.91	0.53	0.41	0.583
	150	1	5	4	75.0	22.32	375	0.0	**1.00**	3.97	1.03	**1.00**	0.89	0.52	0.40	0.586
	200	1	5	3	75.0	22.36	500	0.0	**1.00**	3.95	1.05	**1.00**	0.89	0.52	0.4	0.587
	300	2	10	1	37.5	23.44	750	0.0	**1.00**	3.71	1.07	**1.00**	0.94	0.52	0.41	0.587
	400	1	4	2	74.97	24.48	1000	0.0	**1.00**	2.35	1.92	**1.00**	0.98	0.51	1.03	0.617
	500	1	6	1	59.0	25	1250	0.0	**1.00**	3.3	**1.00**	0.79	**1.00**	0.51	0.42	0.596
100 000	100	1	5	6	75.0	24.13	250	0.0	**1.00**	3.98	1.11	**1.00**	0.97	0.52	1.66	0.586
	150	1	5	4	75.0	23.25	375	0.0	**1.00**	3.97	1.07	**1.00**	0.93	0.52	1.62	0.586
	200	1	5	3	75.0	22.69	500	0.0	**1.00**	3.95	1.04	**1.00**	0.91	0.52	1.59	0.586
	300	1	5	2	75.0	23.08	750	0.0	**1.00**	3.92	1.06	**1.00**	0.92	0.52	1.60	0.587
	400	1	4	2	74.96	13.11	1000	0.0	**1.00**	2.35	1.03	**1.00**	0.52	0.51	2.06	0.617
	500	1	6	1	59.0	25	1250	0.0	**1.00**	3.3	**1.00**	0.79	**1.00**	0.51	1.61	0.597
10 000	100	1	5	6	75.0	23.03	250	0.0	**1.00**	3.98	1.04	**1.00**	0.92	0.52	3.01	0.586
	150	1	5	4	75.0	21.99	375	0.0	**1.00**	3.97	1.01	**1.00**	0.88	0.52	3.03	0.586
	200	1	5	3	75.0	23.68	500	0.0	**1.00**	3.96	1.09	**1.00**	0.95	0.52	2.96	0.586
	300	1	5	2	75.0	22.28	750	0.0	**1.00**	3.92	1.02	**1.00**	0.89	0.52	2.97	0.587
	400	1	4	2	75.0	15.29	1000	0.0	**1.00**	2.35	1.2	**1.00**	0.61	0.51	2.17	0.617
	500	1	6	1	59.0	25	1250	0.0	**1.00**	3.3	**1.00**	0.79	**1.00**	0.51	2.67	0.596
1 000	100	1	5	6	75.0	22.6	250	0.0	**1.00**	3.98	1.04	**1.00**	0.90	0.52	0.69	0.586
	150	1	5	4	75.0	22.11	375	0.0	**1.00**	3.97	1.02	**1.00**	0.88	0.52	0.69	0.586
	200	1	5	3	75.0	22.31	500	0.0	**1.00**	3.96	1.02	**1.00**	0.89	0.52	0.69	0.586
	300	1	5	2	74.94	22.85	750	0.0	**1.00**	3.91	1.05	**1.00**	0.91	0.52	0.66	0.587
	400	1	4	2	75.0	17.29	1000	0.0	**1.00**	2.35	1.35	**1.00**	0.69	0.51	0.31	0.617
	500	1	5	1	59.0	25	1250	0.0	**1.00**	3.3	**1.00**	0.79	**1.00**	0.43	0.56	0.596

Table 5. Energy optimization results.

K (N m^{-1})	V_g (V)	m	n	r	l (mm)	b (mm)	t_p (μm)	t_b (μm)	E_a	δ_a	F_a	L_a	b_a	h_a	η (%)	W ($\times 10^{-4}$)
500 000	100	1	3	8	70.6	25	250	1693	**1.00**	**1.00**	3.53	0.94	**1.00**	0.51	2.74	0.887
	150	1	3	6	68.5	25	375	1183	**1.00**	**1.00**	3.78	0.91	**1.00**	0.51	2.76	0.813
	200	1	3	4	70.6	25	500	1678	**1.00**	**1.00**	3.52	0.94	**1.00**	0.51	2.74	0.885
	300	1	3	2	68.6	25	750	1182	**1.00**	**1.00**	3.77	0.91	**1.00**	0.38	2.74	0.813
	400	1	3	2	70.6	25	1000	1675	**1.00**	**1.00**	3.51	0.94	**1.00**	0.51	2.72	0.885
	500	1	3	2	67.9	24.23	1257	662	**1.00**	**1.00**	3.77	0.91	0.97	0.51	2.61	0.737
100 000	100	1	2	5	73.4	25	260	1049	0.97	1.09	1.49	0.98	**1.00**	0.22	3.53	0.852
	150	2	4	2	37.5	25	375	448	**1.00**	1.14	1.77	**1.00**	**1.00**	0.25	3.48	0.800
	200	1	2	3	75.0	25	500	894	**1.00**	1.15	1.77	**1.00**	**1.00**	0.24	3.49	0.806
	300	1	2	2	75.0	25	750	946	**1.00**	1.12	1.72	**1.00**	**1.00**	0.24	3.48	0.816
	400	1	2	1	68.7	25	1067	1065	0.94	**1.00**	1.16	0.92	**1.00**	0.20	3.43	0.888
	500	1	2	1	74.7	25	1261	1159	**1.00**	1.10	1.50	**1.00**	**1.00**	0.23	3.45	0.874
10 000	100	1	5	4	75.0	25	250	942	**1.00**	3.56	**1.00**	**1.00**	**1.00**	0.50	3.37	0.836
	150	1	5	3	75.0	25	376	592	**1.00**	3.97	**1.00**	**1.00**	**1.00**	0.50	3.45	0.740
	200	1	5	2	74.9	25	507	940	0.99	3.47	**1.00**	**1.00**	**1.00**	0.50	3.32	0.837
	300	2	9	1	37.5	17.6	750	195	**1.00**	2.97	**1.00**	**1.00**	0.70	0.51	2.83	0.691
	400	1	5	1	74.9	25	1001	946	**1.00**	3.47	**1.00**	**1.00**	**1.00**	0.50	3.27	0.839
	500	1	5	1	75	22.16	1250	192	**1.00**	3.67	**1.00**	**1.00**	0.89	0.47	3.19	0.723
1 000	100	1	5	5	74.9	25	250	295	**1.00**	4.21	**1.00**	**1.00**	**1.00**	0.50	0.81	0.657
	150	1	5	3	74.8	25	375	589	**1.00**	3.97	**1.00**	**1.00**	**1.00**	0.50	0.80	0.739
	200	1	5	2	74.8	25	500	939	**1.00**	3.54	**1.00**	**1.00**	**1.00**	0.50	0.72	0.837
	300	1	5	2	74.9	20.7	750	73.2	**1.00**	3.81	**1.00**	**1.00**	0.83	0.53	0.69	0.609
	400	1	5	1	74.9	25	1002	944	**1.00**	3.46	**1.00**	**1.00**	**1.00**	0.50	0.70	0.839
	500	1	5	1	74.9	23.9	1251	377	**1.00**	3.87	**1.00**	**1.00**	0.96	0.50	0.73	0.685

the design problem. As the voltage increases, the minimum thickness of a PZT layer also increases because of the material saturation constraint (equation (38)). This effect, coupled with the fact that the optimizer can only add or subtract PZT thickness one layer at a time (fractional layer thicknesses are not allowed), results in small variations in the optimal weights and efficiencies as the voltage is varied.

Although the applied voltage does not significantly affect the optimized weights and efficiencies, it does affect the physical configuration of the optimized actuator. The low voltage actuator designs (100–200 V) are more complex than the high voltage designs (400–500 V) in the sense that are made up of larger numbers of thinner PZT layers. Increased voltages, therefore, will result in less complex (and thus more

Table 6. Efficiency versus minimum blocked force.

F_b^* (N)	10	15	20	25	30
η (%)	3.79	3.71	3.71	3.68	3.36

easily constructed) arrays, but may adversely affect the power electronics. As the maximum voltage of the drive amplifier increases, so increases the cost, size, weight, and complexity of the amplifier. This optimization example therefore illustrates the trade-off between the recurve array complexity and the complexity of the drive amplifier.

The effect of relaxing the performance constraints is investigated by considering the case of load stiffness $K = 10\,000\ \mathrm{N\,m^{-1}}$ and maximum voltage $V_g = 400$ V for which the blocked force constraint was active. The required minimum blocked force was reduced systematically and the corresponding efficiency recorded in table 6. The value $F_b^* = 10$ N corresponds to an active free displacement constraint. We see that by reducing the blocked force requirement from 30 to 10 N, an increase of the efficiency from 3.36% to 3.79% ($\sim$13% increase) is obtained.

5. Conclusion

In this paper we have presented an optimization formulation for the design of a recurve array. Because of the complexity of the design of a recurve array, this optimization tool has significant advantages as a design tool. Two formulations of the optimization problem were presented. One formulation, weight optimization, is appropriate for applications where weight and/or volume constraints are present. The second formulation, efficiency optimization, is appropriate for applications whose energy sources are limited. The performance of both formulations is demonstrated on a realistic application.

Acknowledgment

This research was supported in part by the Air Force Office of Scientific Research under grant number F49620-01-1-0178.

References

Abdalla M M, Frecker M, Gürdal Z and Lindner D K 2005 Design of a piezoelectric actuator and compliant mechanism combination for maximum energy efficiency *Smart Mater. Struct.* **14** 1421–30

Abdalla M M, Song C, Lindner D K and Gurdal Z 2003 Combined optimization of a recurve actuator and its drive circuit *J. Intell. Mater. Syst. Struct.* **14** 275–86

Brei D, Vendlinski J, Lindner D K, Zhu H and LaVigna C 2003 Development and demonstration of INSTAR—inertially stabilized rifle *Proc. SPIE's Int. Symp. on Smart Structures and Materials: Smart Structures and Integrated Systems (San Diego, CA)* ed E Anderson (Bellingham, WA: SPIE Optical Engineering Press)

Busquets-Monge S, Soremekun G, Hertz E, Crebier C, Ragon S, Boroyevich D, Gürdal Z, Arpilliere M and Lindner D K 2004 Power converter design optimization: a GA based design approach to optimization of power electronics circuits *IEEE Ind. Appl.* **10** 32–9

Chandrasekaran S and Lindner D K 2000 Power flow through controlled piezoelectric actuators *J. Intell. Mater. Syst. Struct.* **11** 469–81

Chandrasekaran S, Lindner D K and Smith R C 2000 Optimized design of switching amplifiers for piezoelectric actuators *J. Intell. Mater. Syst. Struct.* **11** 887–901

Ervin J D and Brei D 1998a Recurve piezoelectric-strain-amplifying actuator architecture *IEEE/ASME Trans. Mechatron.* **3** 293–301

Ervin J D and Brei D 1998b Parallel and serial connections for piezoceramic recurve actuator arrays *Proc. SPIE's—Smart Materials and Structures 1998: Mathematics and Control in Smart Structures (San Diego, CA), Proc. SPIE* **3323** 732–42

Ervin J D and Brei D 2004 Dynamic behaviour of piezoelectric recurve actuation architectures *J. Vib. Acoust.* **126** 37–46

Frecker M 2002 A review of current research activities in optimization of smart structures and actuators *Proc. SPIE's 2002 North American Symp. on Smart Structures and Materials, Modeling, and Signal Processing (San Diego, CA), Proc. SPIE* **4693** 112–23

Kamlah M and Jiang Q 1999 A constitutive model for ferroelectric PZT ceramics under uniaxial loading *Smart Mater. Struct.* **8** 441–59

Lindner D K, Vujic N and Leo D J 2001 Comparison of drive amplifier for piezoelectric actuators *Proc. SPIE—The Int. Soc. Opt. Eng.* **4332** 281–91

Lu X and Hanagud S 2002 An irreversible thermodynamic model of nonlinearities and hysteresis in piezoceramics *43nd AIAA/ASME/AHS/ASC Structures, Structural Dynamics, and Materials Conf. (Denver, CO)* vol 4, pp 2756–65

McMahon M T, Watson L T, Soremekun G A, Gürdal Z and Haftka R T 1998 A Fortran 90 genetic algorithm module for composite laminate structure design *Eng. Comput.* **14** 260–73

Nagendra S, Jestin D, Gurdal Z, Haftka R T and Watson L T 1996 Improved genetic algorithm for the design of stiffened composite panels *Comput. Struct.* **58** 543–55

Smith R C and Ounaies Z 2000 Model for asymmetric hysteresis in piezoceramic materials *Mater. Res. Soc. Symp. Proc.* **604** 285–90